JOURNAL OF MATERIALS SCIENCE 30 (1995) 5561–5575

Review
Corrosion of nickel, iron, cobalt and their alloys in molten salt electrolytes

TZ. TZVETKOFF, A. GIRGINOV*
*Elchem Engineering Laboratory, and *Department of Physical Chemistry, Sofia University of Technology, 1156 Sofia, Bulgaria*
M. BOJINOV
Central Laboratory of Electrochemical Power Sources, Bulgarian Academy of Sciences, 1113 Sofia, Bulgaria

The processes of high-temperature corrosion, anodic dissolution and passivation of nickel, iron, cobalt and their alloys are reviewed to reveal the progress in understanding the reaction mechanisms defined in the last two decades. In the first part, the procedures of thermodynamical analysis of corrosion processes by potential – pO^{2-} diagrams are outlined. The second part is devoted to the electrochemical corrosion, anodic dissolution and passivation of the metals studied, the reaction mechanisms and composition of the corrosion layers formed. The effect of the alloying elements on the corrosion resistance and anodic behaviour of the base metal is treated in the third part. A brief summary of the kinetics of the so-called "hot corrosion" of the studied metals and their alloys in contact with thin molten salt films and aggressive atmospheres is then given. Finally, some conclusions are drawn and some future trends of investigation are indicated.

1. Introduction

Far less attention has been paid to the phenomena of corrosion and passivation of metals in molten salt environments than to the study of their behaviour in aqueous solutions or high-temperature gas systems. With the continuously increasing demand for alloy materials of a new generation working under extreme conditions in modern industry, the study of these processes could provide information of interest both from the fundamental standpoint and from that of the possibly improved application of metals in fused-salt technology.

Corrosion problems in molten salts can be divided in two main groups with respect to the corrosive environment: on the one hand, corrosion of metals submerged in bulk molten salt electrolytes, and on the other hand, the so-called "hot corrosion" most often met in gas combustion systems such as the accelerated corrosion of a metal exposed to an aggressive gas environment and covered by a thin molten salt film. The scientific importance of the first group can be evaluated by studying relatively simple corrosion systems where the main partial cathodic reaction is oxygen anion reduction, the latter being produced either by oxygen dissolved in the melt or from certain dissociation equilibria of molten salt counterions. The fundamental study of the second kind of corrosion provides the possibility of investigating the interaction reactions between thin molten salt films and solid-oxide scales formed on metals via high-temperature oxidation. Last, but not least, the continuous demand for new alloy materials of good mechanical properties combined with the pertinent corrosion resistance, acts as an economic catalyst by which the industrial practice speeds up the investigations in the domain of high-temperature corrosion.

The main purposes of the present review are summarized as follows, from analysis of potential – pO^{2-} diagrams:

1. to obtain comprehensive information on the thermodynamical background of the corrosion of nickel, iron, cobalt and their alloys in molten salt systems;
2. to give an overview of corrosion kinetics of pure nickel, iron and cobalt in a range of molten salt electrolytes with emphasis on the reaction mechanisms and chemical composition of corrosion layers;
3. to define the influence of the major alloying elements in nickel-, iron- and cobalt-based alloys on their corrosion resistance in bulk melts;
4. to present a summary of thermodynamical conditions and kinetics of the so-called "hot corrosion" of nickel and its alloys in contact with thin molten salt films and aggressive atmospheres with particular stress laid on the structure of scales and fluxing mechanisms.

2. Thermodynamical background

2.1. Potential – pO^{2-} diagrams

The regions of immunity, corrosion and passivation of a metal in aqueous solutions can be assessed from the

0022–2461

so-called Pourbaix diagram (potential–pH diagram). Bearing in mind that the oxygen anion was the most likely to be reduced during the partial cathodic reaction, potential – pO^{2-} diagrams were devised in analogy to this treatment for a range of metals in molten salt electrolytes to define the zones of corrosion and passivation. Some representative examples are given below.

2.1.1. Nickel [2–10]

Potential – pO^{2-} diagrams for nickel in molten carbonates [2, 3], nitrates [4, 5], nitrites [6] and sulphates [7–10] were developed. In extending Pourbaix's method to cover molten salts as well, it was necessary to find a function analogous to pH which would express the acidity of the system. It is known that the dissociation of oxygen-containing anions gives rise to a well-defined acid–base behaviour

$$SO_4^{2-} \rightarrow SO_3 + O^{2-} \quad (1)$$

$$NO_3^- \rightarrow NO_2^+ + O^{2-} \quad (2)$$

$$CO_3^{2-} \rightarrow CO_2 + O^{2-} \quad (3)$$

$$2OH^- \rightarrow O^{2-} + H_2O \quad (4)$$

In accordance with the Lux–Flood theory, oxygen-containing anions act as a base in the supply of oxide anions and the corresponding gas oxides are their conjugate acids. From the above equilibria it follows that the acidity of the melt may be expressed either by pO^{2-} or by $-\log p_{gas}$. Accordingly, the E/pO^{2-} diagram provides a suitable framework for the electrochemical behaviour of different metals. Such a diagram for nickel in fused Na_2SO_4 at 973 K proposed by Gribaudo and Rameau [9] is presented in Fig. 1. The diagram at 1173 K given by Sequeira and Hocking [8] is, in principle, analogous to the one presented.

The assumption that the occurrence of corrosion implies an overall activity of ions $> 10^{-6}$ M allows some predictions. The area of corrosion is distinguished at high potentials and low oxygen ion activity. The passive region comprises the oxide NiO and two sulphides, NiS and Ni_3S_2, extending over the whole range of pO^{2-}. Herein the passivation concept could be misleading because sulphides especially are unlikely to give effective protection. The NiO area extends at potentials above the O_2/O^{2-} line, i.e. passive film breakdown can occur via oxygen discharge (transpassivity). In basic melts the fluxing of the oxide scale by oxide ions can lead to the formation of soluble species (e.g. NiO_2^{2-}) accelerating metal corrosion instead of passivation. It should be noted that this theoretical treatment is not obligatorily relevant under the influence of morphology, solubility and kinetic factors.

2.1.2. Iron [9–13]

The theoretical background of the Pourbaix-like diagrams of iron in fused NaOH–KOH takes into account Equilibrium 4 and thus variations in acidity correspond to variations in the O^{2-}/H_2O ratio. The acidity influences the oxidation/reduction of hydroxides: reduction in acidic media leads to H_2 formation, whereas in strongly basic melts, H^- is formed; oxidation of OH^- gives superoxides in acidic and peroxides in basic media. The potential – pO^{2-}/pH_2O diagram of iron [12] in fused NaOH at 350 °C is presented in Fig. 2.

The major conclusion is that the sole domain of iron solubility in NaOH is the strongly basic one, corresponding to the capacity of Fe(III) reduction.

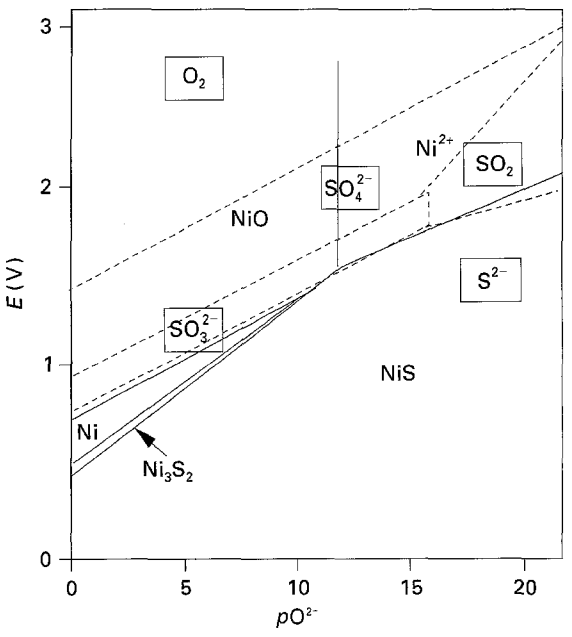

Figure 1 Potential – pO^{2-} diagram for the Ni/Na_2SO_4 system at 973 K (after Gribaudo and Rameau [9]).

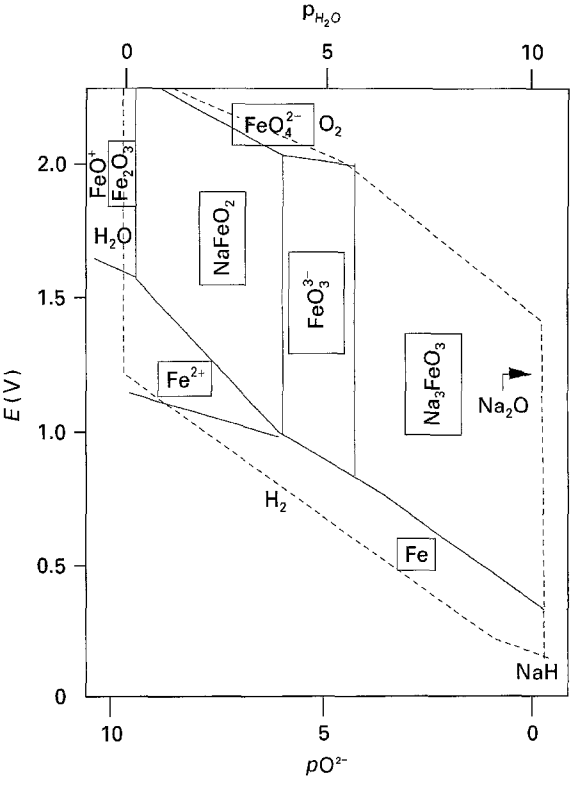

Figure 2 Potential – pO^{2-}–pH_2O diagram for iron in fused NaOH at 523 K (after Doisneau and Tremillon [12]).

A weak solubility region exists in a strongly acidic medium in the presence of H_2O under the form of FeO^+ or Fe^{2+} (in contact with Fe_3O_4 solids). Finally, iron could dissolve as ferrate(VI) in a neutral and extremely oxidizing medium (peroxide + oxygen). The composition of the passive layer on iron is quite complicated and strongly dependent on oxoacidity (Fig. 2). It comprises a range of pure and mixed iron oxides (Fe_2O_3, Fe_3O_4, $NaFeO_2$, Na_3FeO_3). The E/pO^{2-} diagram of iron in sulphate [9] also shows the stability regions of FeO and the iron sulphide, FeS. In the diagram, for iron in $NaNO_3/NaNO_2$ mixtures [13] at low pO^{2-} (basic media), a $Na_4Fe_2O_5$ region is detected. A good correlation was established between the diagram predictions and corrosion tests reported in the literature. Therefore, the thermodynamic studies allow a better understanding of the corrosion and nature of oxide layers formed in different molten salt mixtures.

3. Overview of electrochemical corrosion of nickel, iron and cobalt in molten salts

3.1. Nickel [14–66]

3.1.1. Chloride electrolytes [14–22]

Alkali chloride-based electrolytes are commonly used for electrodeposition of metals and alloys from molten media. Thus several studies of the electrochemical behaviour of nickel have been attempted. Kochergin *et al.* [18] determined the stationary potentials (versus a Pb^{2+}/Pb reference) and the corrosion rate of nickel and low-carbon steel in KCl, as well as in equimolar NaCl–KCl, $MgCl_2$–KCl, $CaCl_2$–KCl and $BaCl_2$–KCl mixtures at 850 °C. The main conclusions from their work are that in pure KCl the rest potential is more negative, and the corrosion is higher than in KCl–NaCl, due to the greater stability of $MeCl_4^{2-}$ ions in the melt. In the Mg–Ba range the corrosion rate was reduced, although the rest potentials were shifted to more negative values (a possible explanation is the increase of the dissociation energy of the Me–Cl bond in the Mg–Ca–Ba range). Nickel proved to be nobler than titanium, chromium and stainless steels in these media [18].

Feng and Melendres [20] showed that the anodic dissolution of a range of metals (iron, cobalt, nickel, molybdenum) in the pure LiCl–KCl eutectic at 375–470 °C followed pseudo-Tafel lines for several decades of the current. The addition of oxide ions allowed the exhibition of typical passivation features [20]. Passivation was reversible for iron, cobalt and copper, partially irreversible for nickel and completely irreversible for molybdenum [20]. Zhbanov *et al.* [21] measured rest potentials of approximately − 2 V versus the chlorine reference for nickel in equimolar KCl–KF mixtures at 700–800 °C. Three regions could be distinguished in the polarization curves: an induction period during which the current equalled the corrosion one, followed by a Tafel region stretching over two decades of the current and a limiting diffusion current [21]. At higher current densities, nickel dissolved without any polarization due to the accumulation of molten $NiCl_2$ near the surface. The mean valency of nickel dissolution was estimated to be 2. In chloride–fluoride melts, that parameter increased due to stronger complexability [21]. Nishikata and Haruyama [22] found that both the rest potentials and the corrosion rate of nickel and its alloys in molten NaCl–KCl were of the same order of magnitude. Anodic polarization curves for nickel in aerated NaCl–KCl exhibited a pseudo–Tafel behaviour with no traces of passivation at least for current densities lower than 0.1 A cm^{-2} [22]. A summary of the corrosion kinetics of nickel in halide and oxyhalide melts is presented in Fig. 3.

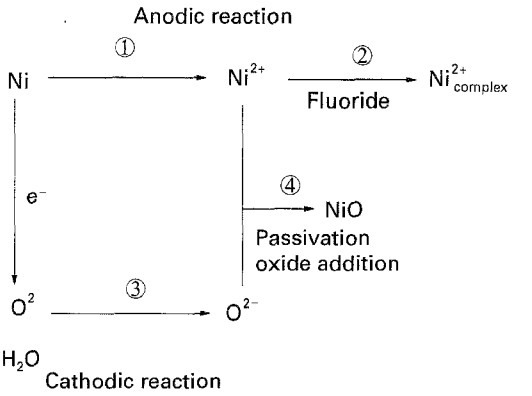

Figure 3 Summary of the electrochemical corrosion reactions of nickel in halide melts.

3.1.2. Nitrate electrolytes [23–26]

The study of anodic dissolution of metals in concentrated ionic solutions at high current densities is relevant in electromachining. The phenomenology of the corresponding processes is closely related to the dissolution of passivated metals through an oxide film. A kinetic model of iron, cobalt, and nickel anodization in fused nitrate was proposed [23, 24] taking into account three processes – the formation of the passive film, electrodissolution of the uncovered metal and electrodissolution of metal by transport through the passive film. The rate of the passive film formation via two-dimensional nucleation and growth coupled with a diffusional contribution was expressed at a constant potential as

$$I_{\text{film}} = K_1 t^2 \exp(-t^3/\tau^3) \quad (5)$$

where $\tau = 3/\pi V^2 N$, $K_1 = q_m V^2 \pi N$, q_m is the charge of the monolayer formation, N is the nucleation rate constant, and V the rate constant of growth. The film-free dissolution at certain centres is described as follows

$$I_{\text{diss}} = I_0 \exp[-(\pi/3) V^2 N t^3] \quad (6)$$

and finally, the dissolution of metal through the film resulted in

$$I_{\text{fdiss}} = I'_0 \{1 - \exp[-(\pi/3) V^2 N t^3]\} \quad (7)$$

If metal was prepassivated, the mechanism could be simplified, because $I_{\text{fdiss}} \ll I_{\text{diss}}$ and according to podesta *et al.* [24] the potentiostatic transients can be

described by the equation

$$I = K_1 t^2 \exp[-t^3/\tau^3] + I'_0\{1 - \exp[-(\pi/3)V^2 N t^3]\} \quad (8)$$

reproducing the experimental results for iron, cobalt and nickel in fused (Li, Na, K) NO_3 eutectic [24]. The authors concluded that the transpassivity process required the rupture of the passive film formed and was thus related to the localized corrosion.

The effect of phosphate and chromate addition as Lux–flood acids, and peroxides, hydroxides and carbonates as bases on the corrosion mechanism of nickel in (Na, K) NO_3 melts, was characterized by Baraka and Baraka [25, 26]. In acidic melts the anodic oxidation proceeded via the reaction sequence 1–2 outlined in Fig. 4.

The oxygen anions were produced by equilibrium 3 (Fig. 4) and the resulting nitronium ions were reduced via the cathodic coupled reaction 4 (Fig. 4). The addition of phosphate to the melt led to the formation of a thick corrosion layer of nickel phosphates. In general, acidic melts produced increased corrosion rates due to the interaction between the metal and nitronium ion [25]. On the other hand, basic melts would enhance the passivation of the metal and promote its behaviour as a metal/metal oxide electrode (reaction 2 in Fig. 4).

If reactions 1 and 2 (Fig. 4) were rate determining, a Tafel law would govern the kinetics [25]

$$\eta = \text{const} - ap\mathrm{O}^{2-} - b\log i \quad (9)$$

and if oxygen evolution on NiO was rate determining

$$\eta = \text{const}' - ap\mathrm{O}^{2-} - b\log i \quad (10)$$

i.e. a linear relationship between polarization and pO^{2-} was obtained in agreement with the polarization decreasing as basicity increased [25].

In a further paper by the same authors [26], the effect of halide ions addition on the corrosion behaviour of nickel in nitrate melts was investigated. The observed experimental variation of the rest potential, weight gain and anodic polarization with halide ion concentration were tentatively explained by the suggestion that the halide ions were oxidized by nitrate according to the reaction sequence 3–6 (- - - in Fig. 4). The elemental halides (especially bromine and iodine) were assumed to catalyse the potential determining

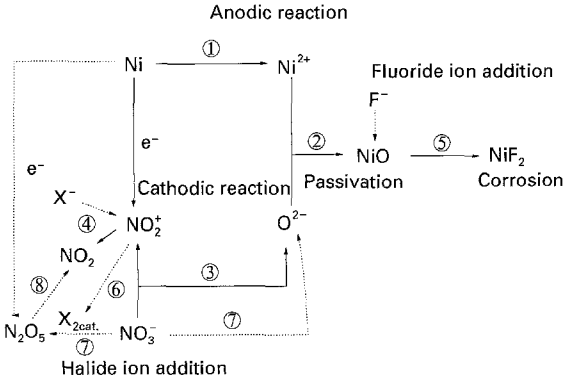

Figure 4 Summary of the electrochemical corrosion reactions of nickel in nitrate melts. (- - -) Effect of halide addition.

Reaction 7 in the melt, shifting the potential to negative values. Namely, iodine acted as a corrosion inhibitor in analogy to aqueous environments [26]. The effect of fluoride addition was markedly different [26]: nickel corrosion was increased through the penetration of the NiO passive film and the metal oxidation of NiF_2 (reaction 5).

3.1.3. Sulphate electrolytes [27–37]

Sequeira and Hocking [35, 36] observed nickel passivation via NiO formation in pure molten Na_2SO_4. Passivation was preceeded by active dissolution of the metal as per the general diagram depicted in Fig. 5a.

Nickel had a mixed potential between the anodic Reactions 1 and 2 and the cathodic coupled reaction sequence 3 and 4 (Fig. 5a). The authors [35] concluded that the same primary step 1 acted as a common precursor to both the active dissolution 2–2′ and the passivation 5–6 (Fig. 5a) where Ni–SO_3 represented a chemisorbed surface complex.

The reactions in the transpassive region which resulted in further nickel corrosion and oxygen evolution were explained by the author [35] by the consecutive steps 7–9 (Fig. 5a).

The effect of NaCl addition can be summarized as follows [35]: (1) shift of the characteristic potentials of the polarization curves to the anodic direction; (2) increase of the critical passivation current; (3) no significant effect on the passive region, and (4) transpassive current smaller in NaCl-containing melts. To explain these features, the reaction sequence 10–12 was proposed (Fig. 5a):

(a) equilibrium 10 (Fig. 5a) was displaced to the right by the NaCl addition;

(b) formation of a nickel sulphide layer (reaction 11);

(c) dissolution and oxidation of sulphide by oxygen evolved on passive and transpassive nickel (reaction 12) with simultaneous passivation.

The influence of SO_3 (gas) was also studied [35] and a brief summary is given below: (1) the increased SO_3 partial pressure led to the initiation of passivation; (2) the effect is more pronounced for preoxidized nickel samples in an SO_3 atmosphere.

Most of the results were confirmed by surface analysis in a subsequent paper [36] – both NiO and a Ni_3S_2 sublayer were identified together with a Ni–Ni_3S_2 eutectic structure (Fig. 5b). Nishikata and Haruyama [22] demonstrated that nickel dissolved through the oxide film in (Li, K)$_2SO_4$ melts. Sulphate oxidation occurred at very positive potentials on the passive nickel surface [22]. Abou–Elenien [37] established that the corrosion current densities of nickel increased with the SO_2 concentration [37]. The role of SO_2 cannot be separated from that of SO_3. Both the metal nobility and the formation of a coherent oxide layer affected the corrosion rate in molten sulphates [37].

3.1.4. Carbonate electrolytes [38–47]

The corrosion and anodic behaviour of a range of metals in molten carbonates were studied in relation

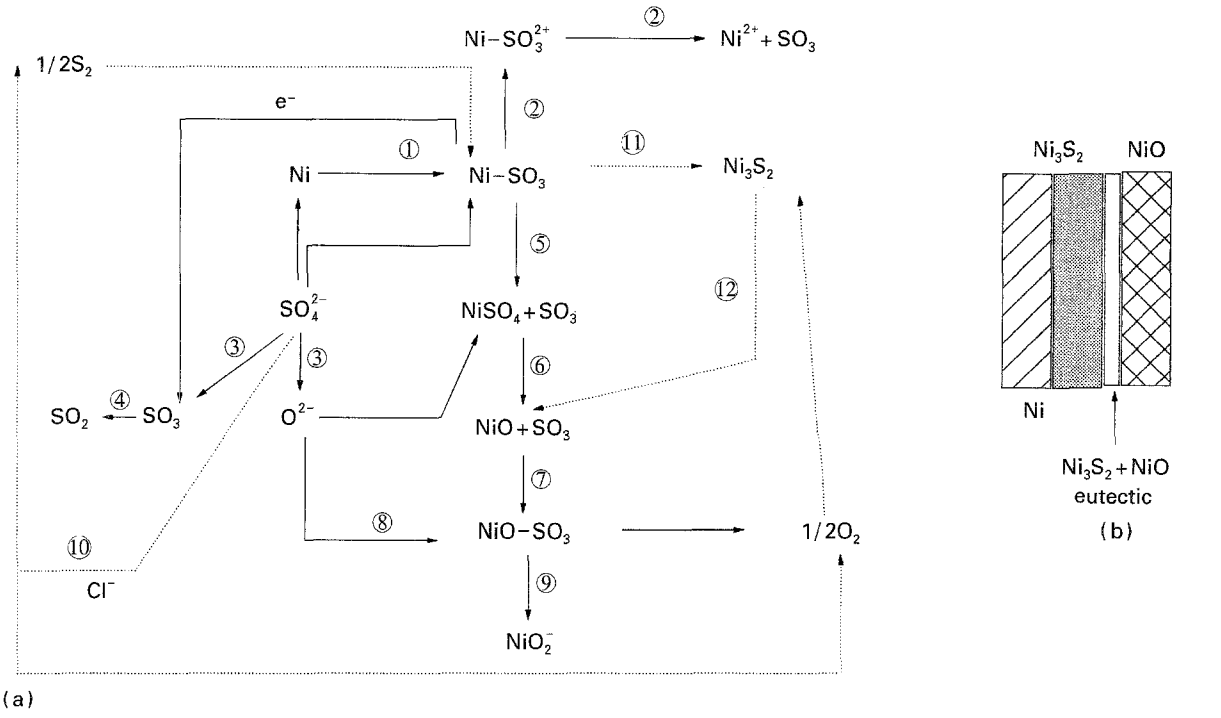

Figure 5 (a) Summary of the electrochemical corrosion reactions of nickel in sulphate melts. (- - -) Effect of halide addition. (b) Structure of the anodic layer formed on nickel in mixed sulphate–chloride melts.

to the operation of high-temperature fuel cells. Devereux and co-workers [40–44] contributed greatly to the understanding of corrosion and anodic oxidation of nickel in carbonate melts. A numerical procedure for the analysis of complex polarization curves [41] was applied in the study of the corroding nickel electrode in Na_2CO_3 melt in a CO/CO_2 atmosphere of various compositions. The procedure was based on the model approaches of Vetter and treated the total current at any potential as a sum of the partial anodic and cathodic current densities of individual processes assumed to take place under reaction–diffusion control. Passivation was taken into account simply by assuming the independence of current above a certain critical value of the potential [43]. By comparing the environmental dependence of empirical model predictions for the individual reaction with theoretical candidates, a total of four anodic and one cathodic reactions were suggested to run on nickel in carbonate. These reactions are depicted in Fig. 6a. The existence of NiO and possibly of Ni_2O_3 was confirmed by X-ray diffraction studies [43].

During the study of anodic oxidation of nickel in carbonate melts, Iyer and Devereux [44] found a peculiar type of corrosion attack, namely liquid-line corrosion of nickel. The following reaction sequence was proposed to explain the phenomenon. Anodic oxidation was preceeded by the injection of cation vacancies at the oxide/melt interface (reactions 1–2, Fig. 6b). Dissolution of the scale took place at the film/solution boundary (reaction 3, Fig. 6b).

The authors [44] assumed that the liquid-line corrosion attack was limited by the cathodic reaction – oxygen reduction via peroxide or superoxide formation (reactions 4–5, Fig. 6b). If the oxygen reduction was limited by the charge transfer [44], the oxygen flow was proportional to the exchange current

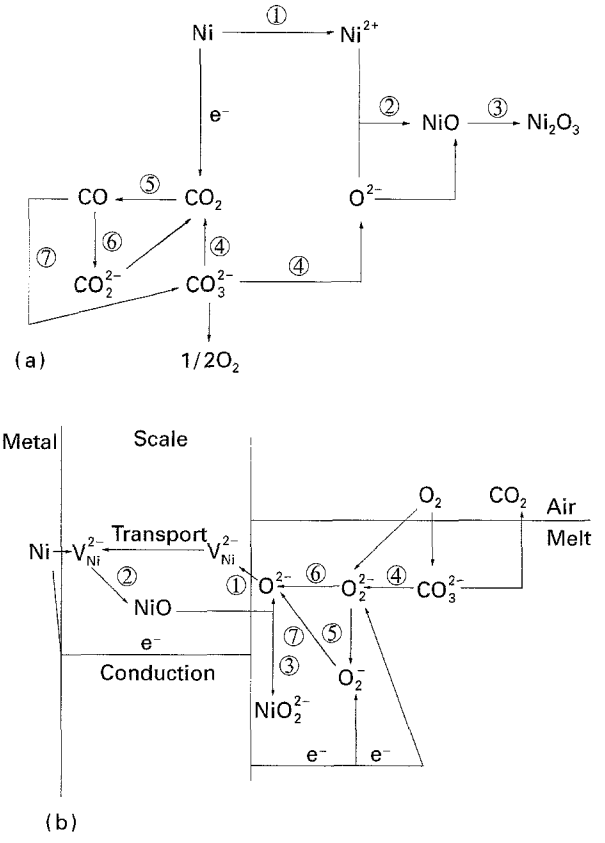

Figure 6 (a) Summary of the electrochemical corrosion reactions of nickel in bulk carbonate melts. (b) Liquid–line corrosion of nickel in carbonate melts.

density

$$J \propto i_0 = kc_0 \exp[(\alpha z F/RT)E_r] \qquad (11)$$

For peroxide reduction [44]

$$J' \propto i_0 \propto P^{-(1/2+3\alpha/4)} a_{CO_3^{2-}}^{(1+\alpha/2)} \qquad (12)$$

and for superoxide reduction

$$J'' \propto i_0 \propto P^{(1-3\alpha)/4} a_{CO_3^{2-}}^{(1+\alpha)/2} \quad (13)$$

The authors [44] suggested a simplified model of the corrosion process in which the depth of the attack was described by a parabolic equation

$$X^2 = aVnJt \quad (14)$$

where V is the molar volume of nickel, $n = 2$, $a \approx 0, 12$ (geometrical factor). For a constant J, the $X/t^{1/2}$ dependence expected was in accordance with the experimental results [44]. The empirically derived pressure dependence of J corresponded to that predicted by Equation 12, i.e. the peroxide formation was probably the limiting stage of the corrosion process [44].

3.1.5. Hydroxide electrolytes [48–53]

Nickel corrosion in molten alkali hydroxides was the subject of a series of investigations due to the possible use of the metal as a base material for high-temperature reactors and baths. In early work [48, 49] the following general corrosion reaction was proposed

$$Ni + 2NaOH \rightarrow Na_2NiO_2 + H_2 \quad (15)$$

Budnik and Zarubitskij and Zarubitskij *et al.* [51, 54] showed that during nickel corrosion in hydrated NaOH–KOH melts at 200 °C, the frequency dependence of the electrochemical impedance was consistent with the impedance of a film-covered electrode (most probably by NiO). The potential dependence of both active and reactive impedance components illustrated the possibility of NiO transformation into higher valency nickel oxides. The open circuit evolution of the electrode impedance following anodic polarization was explained by the oxygen exchange at the electrode surface [51]. A further study of the same authors [54] gave evidence of the formation of a corrosion layer of NiO by X-ray diffraction. Thermogravimetric analysis [54] showed that, besides Na_2NiO_2, higher valency nickel compounds are formed. The limiting stage of the process appeared to be either the NiO/Na_2NiO_2 transformation or the nickelate dissolution in the melt [54]. Owing to its higher ability to dissolve oxygen, KOH was proven to be more aggressive towards nickel than NaOH [54].

Tzvetkoff and co-workers [52, 53] studied the corrosion of a range of metals and alloys in fused alkali hydroxides in relation to the high-temperature descaling processes, and showed that nickel was the most resistant material in fused NaOH. A thin, well adhering and continuous passive film of fair protective ability was formed on the metal surface [52]. The addition of $NaNO_3$ to the melt was found to be detrimental at low concentrations and to help passivation at higher contents in accordance with [55]. The addition of small quantities of NaF tended to decrease the corrosion rate of all the metals studied. Nickel corrosion in NaOH was further studied in varying atmospheric conditions using X-ray and electron diffraction [53]. A primary corrosion layer was found to be mostly NiO (lattice constant 0.421 nm [53]). X-ray and chemical analyses of secondary corrosion products evinced the presence of $Ni(OH)_2$ [53] formed via hydrolysis by water steam

$$Na_2NiO_2 + 2H_2O \rightarrow Ni(OH)_2 + 2NaOH \quad (16)$$

Corrosion rates of nickel were found to be strongly affected by the atmospheres [53]: (1) peroxide content depended on the partial pressure of oxygen; (2) water steam produced a decrease of peroxide content having an inhibiting effect. Na_2O_2 addition to NaOH melt enhanced drastically the corrosion, even in nitrogen atmosphere [53], thus being in confirmation of the main cathodic coupled reaction (oxygen reduction [53]).

3.1.6. Other molten electrolytes (sulphides, molybdates, fluorides, borates, phosphates) [56–64]

The corrosion rate of nickel and cobalt in sulphide concentrates from copper extraction was found to be rotation-speed dependent, i.e. was transport limited [56]. This finding was confirmed by the apparent activation energies of the order of 30–40 kJ mol^{-1} determined [56]. The rate of nickel dissolution was two to three times higher than that of cobalt, being higher in the real concentrate and lower in synthetic Cu_2S/Ni_3S_2 molten mixtures.

Liu and Devereux [57] interpreted the linear polarization plot of nickel in Na_2S–FeS melts in terms of ohmic hindrances of the dissolution process. Weight loss measurements gave a linear corrosion rate ($K = 1.6 \times 10^{-6}$ g cm^{-2} s^{-1}) and were associated with the chemical dissolution of nickel

$$Ni + H_2S \rightarrow NiS + H_2 \quad (17)$$

Estimates of the exchange current density ($\geqslant 0.25$ A cm^{-2}) were obtained from the activation term of the electrode polarization [57]. The anomalous excess weight loss in the longer exposure time experiments was attributed to trace polysulphide

$$Ni + S_2^{2-} \rightarrow Ni^{2+} + 2S^{2-} \quad (18)$$

Ustinov and co-workers [58, 59] suggested the basic corrosion reaction of nickel in molybdate melts to read

$$Ni + MoO_3 \rightarrow NiO + MoO_2 \quad (19)$$

and the secondary one as

$$Ni + \tfrac{1}{2}O_2 \rightarrow NiO \quad (20)$$

The weight loss in prolonged exposure could be due to the acid fluxing of the NiO scale with MoO_3 [59]

$$MoO_3 + NiO \rightarrow NiMoO_4 \quad (21)$$

One of the most widely used reference electrodes in LiF–KF–NaF melts (FLINAK) is the Ni/NiF_2 electrode. Robin and Lepinay [63] used convolutional voltammetry to assess the kinetics of iron and nickel dissolution in FLINAK at 600 °C. The standard potential E_x^o (Ni/Ni(II)) was estimated to be 2.16 ± 0.01 V versus K^+/K reference electrode using the diffusion coefficient of Ni(II) (4.5×10^{-6} cm^2 s^{-1})

determined elsewhere [61]. The theoretical value (2.29 V) was more positive than the calculated one, due to the complexation of Ni(II) probably in the form of NiF_6^{4-}. Semi-integration analysis [63] showed that reversible anodic dissolution occurred via the two-electron reaction

$$Ni \rightarrow Ni(II) + 2e^- \quad (22)$$

Anodic polarization curves of nickel in phosphate and borate melts exhibited four regions [64]: anodic dissolution of nickel, oxygen evolution and passivation by NiO formation, passive state (NiO growth) and oxygen evolution on the passive nickel anode [64]. The transition from cyclic to linear chain borates led to the increase of the critical passivation current. The average corrosion rate of nickel increased in the range $NaPO_3$–$NaBO_2$, $NaPO_3$–$Na_2B_4O_7$, $NaPO_3$–NaB_5O_8. The increase of the $NaPO_3$ content in borax melts resulted in the increase of the critical current due to the ability of metaphosphate to dissolve NiO. Thus the rate of nickel corrosion in phosphate mixtures was about two times higher than in mixed phosphate–borate melts [64].

3.2. Iron and cobalt [20, 22–24, 37, 52, 56, 63, 65–85]

3.2.1. Halide electrolytes [20, 22, 63, 65–69, 85]

Pure iron is a rarely used construction material in a molten salt medium, and studies of its behaviour are limited. Iron oxidation in LiCl–KCl eutectic with and without Li_2O addition was studied by Feng and Melendres [20]. Anodic dissolution with a Tafel slope of ~ 0.1 V/decade was measured for iron in the pure eutectic, the departure from linearity suggesting the mixed control of the process [20]. Cathodic and anodic portions of voltammetric waves showed the fine structure of multiple peaks which indicated passivation reactions with the multilayered films obtained. The rate of initial film formation appeared to be a dissolution–precipitation process complicated by a chemical reaction (presumably formation of Fe(II) chloride complexes). Film growth was probably governed by a high-field-assisted migration [20]. Reduction of anodic passive films on iron in LiCl–KCl–Li_2O seemed to be a two-step process suggestive of some divalent compound of iron in the film [20]. Anodic dissolution of iron in NaCl–KCl melts in an air atmosphere presented the Tafel behaviour with no sign of passivation at least for current densities smaller than 0.1 A cm^{-2} [22]. Tzvetkoff [69] found that the addition of F^- to chloride melts inhibited the corrosion process, whereas small quantities of NO_3^- led to higher corrosion, the effect being the opposite for larger amounts of NO_3^- added [69]. Robin and Lepinay [63] were able to compute the standard potential of the Fe(II)/Fe couple in FLINAK (1.75 $\pm$ 0.01 V versus K^+/K reference electrode). Complexation of Fe(II) as FeF_6^{4-} was suggested [63], the theoretical values of the potential being more positive than those calculated.

Orchard and Mamantov [85] determined the open-circuit potential of cobalt in the $AlCl_3$–NaCl melt (0.92 $\pm$ 0.02 V versus Al(III)/Al reference). Two anodic processes and one cathodic were observed, the transitions related to the passage of a certain quantity of charge through the interface (associated with the surface film formation [85]). In non-saturated melts only one anodic process was detected [85]. Spectro-electrochemical studies demonstrated that $CoCl_4^{2-}$ was the main soluble species [85]. Mass balance showed that a substantial fraction of oxidized cobalt was present as a solid [85]. A two-step mechanism was proposed to cover the reaction sequence [85]

$$Co + 2Cl^- \rightarrow CoCl_2 + 2e^- \quad (23)$$

$$CoCl_2 + 2Cl^- \rightarrow CoCl_4^{2-} \quad (24)$$

Continuous anodization led to precipitation of $CoCl_4^{2-}$ from the melt [85].

3.2.2. Other molten electrolytes (nitrates, nitrites, carbonates, hydroxides, etc.) [70–82]

Arvia and co-workers [70, 72, 73, 75] confirmed the validity of the simplified model above in reference to the nickel passivation in fused nitrates also in the case of iron and cobalt.

Kozhemjako *et al.* [77] found that iron passivated in KOH melts at 470 °C. A reaction sequence based on standard potentials of redox couples was proposed [77]

$$Fe + O^{2-} \rightarrow FeO + 2e^- \quad (25)$$

$$2Fe + 3O^{2-} \rightarrow Fe_2O_3 + 6e^- \quad (26)$$

$$Fe + 2O^{2-} \rightarrow FeO_2^- + 3e^- \quad (27)$$

The increase of pO^{2-} via the reduction of O_2^{2-} and O_2^- resulted in the formation of soluble ferrites and ferrates [77].

Tzvetkoff [78] pointed out the formation of Fe_3O_4 on iron in fused NaOH at 480 °C [78]. Corrosion rates in 100% O_2 were five times higher than in 1% O_2–99% N_2 atmosphere [78]. Water steam played the role of an inhibitor inducing the 70% reduction of corrosion [78]. The rate of interaction of Fe_3O_4 with the melt was greater than that of Fe_2O_3, and again water steam slowed down the dissolution rate of oxides [78].

Azzi and Rameau [79] demonstrated that the corrosion rate of iron in $(Na, K)_2CO_3$ was limited by the diffusion of oxidizing species through the corrosion product rather than in the melt [79]. Oxidizing species were dissolved CO_2 according to the mechanism outlined in Fig. 7, reactions 3 and 4.

Oxygen participated indirectly in corrosion by O_2^{2-} formed via equilibrium 5 (Fig. 7) and reduced to oxygen anions [79].

Penjagina *et al.* [83, 84] found that cobalt was less susceptible to passivation than nickel and iron. In a CO_2 atmosphere, the dissolution proceeded at lower temperatures, passivity being reached at higher ones

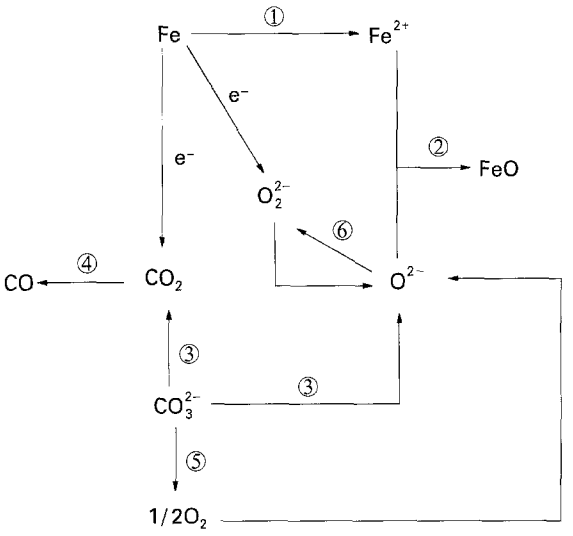

Figure 7 Summary of the electrochemical corrosion reactions of iron in carbonate melts.

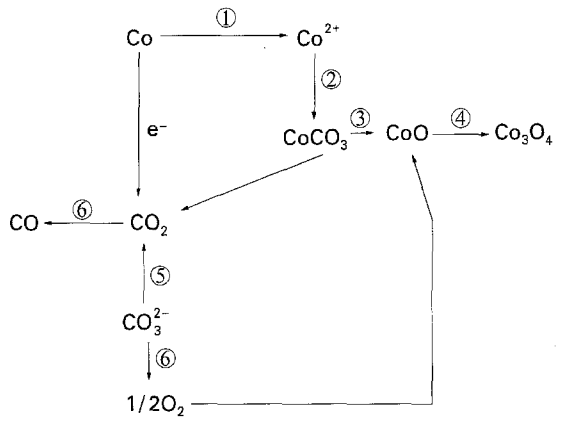

Figure 8 Summary of the electrochemical corrosion reactions of cobalt in carbonate melts.

(> 700 °C). The current in the passive state was three orders of magnitude lower than the critical current [83]. Cobalt corrosion was practically absent without O_2 in the system; at low anodic polarizations, cobalt passed into the solution at a mean valency of 2 [83]. The reaction sequence proposed to explain the anodic behaviour of cobalt in carbonates [83] is given in Fig. 8, with oxide Co_3O_4 as the main passivation product [83].

3.3. Iron, nickel and cobalt-based alloys [22, 50, 64, 86–97]

The investigations of the corrosion and anodic behaviour of alloys in molten media are relatively scarce. Thus the effect of the main alloying elements on the corrosion rate will be briefly discussed. A review of early literature was presented by Inman and Wrench [97].

3.3.1. Halide electrolytes [22, 64, 86–88]

Nishikata and Haruyama [22] demonstrated that chromium in an amount of 5–15 wt% considerably decreased the corrosion current density of nickel and inhibited its anodic dissolution due probably to the formation of some chromium oxide on the surface [22]. Molybdenum in nickel alloys had a smaller impact on the corrosion rate but a greater one on the anodic dissolution [22]. Belov *et al.* [86] demonstrated that the nickel additive in stainless steels lowered the corrosion rate and shifted the rest potential to the positive.

The only study (to our knowledge) of stress corrosion cracking of a 304L steel in NaCl–$CaCl_2$ melts was attempted by Atmani and Rameau [88]. Both square-wave and creep tests showed that depassivation/passivation occurred in molten chlorides [88]. In oxygen atmospheres, the tensile stress, σ_R, increased with the elongation rate (being a constant in inert atmospheres [88]). Two critical elongation rates were defined: no further variation was produced above 0.01 mm s^{-1}, and a transition between the ductile-type cracking and the embrittle-type behaviour was observed at 10^{-5} mm s^{-1} [88]. Between the two critical values, stress corrosion cracking and mechanical breaking took place simultaneously [88].

3.3.2. Nitrate electrolytes [89–91]

Baraka *et al.* [89] revealed the formation of a passivating film of Fe_3O_4 mainly during corrosion of mild steel in (Na, K)NO_3 eutectic at 250–450 °C [89]. Film thickening proceeded according to a parabolic law with an activation energy of 71.3 kJ mol^{-1} [89]. Doelling *et al.* [90] investigated the effect of the NaCl additive on pitting corrosion of St37 in the (Na, K)NO_3 eutectic. Anodic polarization curves revealed three plateaus separated by Tafel regions [90] probably due to Fe_3O_4, Fe_2O_3 formation, nitrite and nitrate oxidation, respectively [90]. During pitting in NaCl-containing melts, a non-linear dependence of both pitting and repassivation potentials on $\log c_{Cl^-}$ was observed [90]. Pit growth followed an approximately cubic law [90].

Nijger *et al.* [91] showed that low-carbon steels in KNO_3–$Mg(NO_3)_2$ eutectic suffered from localized corrosion. For the chromium-containing steel, the increase of carbon content led to the increase of the corrosion rate. An analogous impact of the manganese additive was detected [91]. A considerable increase of the corrosion rate was observed in melts containing more than 0.5% NaCl [91]. Austenitic stainless steels exhibited a four to five times lower corrosion rate which was not influenced by the addition of NaCl to the electrolyte [91]. A protective chromium–iron oxide scale was formed on Cr–Ni containing steels; on the austenitic ones, the spinel type scale improved the corrosion resistance of the substrate [91].

3.3.3. Sulphate electrolytes [87, 92–94]

An investigation of corrosion of nickel alloys containing carbides of titanium, zirconium, hafnium vanadium, niobium and tantalum in molten Na_2SO_4–NaCl mixtures was carried out by Dmitrieva *et al.* [87]. HfC and ZrC additives seemed to ensure

better corrosion resistance than pure nickel, whereas the other carbides had a negative impact (most pronounced with TiC) [87]. X-ray microanalysis showed that nickel and oxygen were evenly distributed; titanium was mostly in the carbide inclusions. The basic phases determined in the corrosion layer were NiO, Ni_3S_2 in the nickel-containing part, as well as $NaTaO_3$, $NaNbO_3$, $NaVO_3$, VO_x, TiS_x shaping the cathodic areas [87].

Schendler and Schwenk [92] divided the anodic oxidation of Cr–Ni containing steels and Inconel in the ternary $(Li, Na, K)_2SO_4$ eutectic melt into three regions: active, passive and transpassive dissolution. Basically, five types of corrosion products were detected: I, inner layer containing oxides and sulphides (Ni–Cr–Ti steels, TiS_2, Cr_2O_3 and Cr_2S_3); II, no inner layer, porous oxides and sulphides (24%Cr steel, Cr, S, O layer); III, film of minor elements (Inconel, $Ni_{60}Cr_{23}$, active dissolution, Cr, S, O + Fe and Mn); IV, Inconel, transpassive region, sulphides and oxides of iron, nickel, chromium, vanadium–two layer structure of sulphides and oxides (Ni–Cr–Ti steels, passive region). The authors [92] concluded that inner sulphidation and two-layered films were typical both for the active and the transpassive dissolution (active dissolution being stimulated by reduction of SO_4^{2-} to S^{2-}, and the transpassive state by oxidation of SO_4^{2-} to SO_3 and O_2) [92]. Erdoes *et al.* [93] defined in a $(Na, K)_2SO_4$ melt, the resistant alloys forming Cr_2O_3 and TiO_2 scales and the non-resistant ones with scales based on NiO, Ni_3S_2 and Ni–Cr spinel phase [93]. Quasi-stationary current versus potential curves had a certain range of passivity due to the protective layer of Cr_2O_3 with unevenly distributed Cr_2S_3 particles; transpassivity resulted in the abundance of Cr_2S_3 [93]. The results were explained on the basis of a simple anodic reaction $Me \rightarrow Me^{n+} + ne^-$ and Lux–Flood equilibria of the type

$$SO_4^{2-} \rightarrow SO_3 + 1/2O_2 + O^{2-} \quad (28)$$

$$SO_4^{2-} \rightarrow SO_2 + 1/2O_2 + O^{2-} \quad (29)$$

In the same paper [93] the preliminary investigation of cobalt-based alloys indicated that their corrosion resistance could be associated with $Cr_2O_3 + WS_2$ scale formation, and alloys susceptible to corrosion did form cobalt-based oxide layers (CoO, $(Co, Ni)_9S_8$, $CoCr_2O_4$, etc.).

Gribaudo and Rameau [94] showed that AISI310 steel in $(Li, Na)_2SO_4$ melts featured additional voltammetric peaks as compared to the ones at a platinum electrode. In an attempt to identify these peaks, the polarization curves of Fe(II), Fe(II)/(III), Cr(III) and Ni(II) on a platinum electrode were registered [94]. It was found that the rest potential was situated between the reversible ones for Fe(II)/Fe and SO_4^{2-}/SO_3^{2-}, indicating the mixed potential of general corrosion of stainless steel [94]. In principle, the localized corrosion was to be expected with a chromium-depleted zone being inferior to the austenitic matrix [94]. $M_{23}C_6$ and M_7C_3 were the most anodic phases and corroded preferentially. Silicon addition involved the formation of SiO_2 in the protective layers, decreasing the rate of general corrosion but with no effect on local corrosion [94]. Tungsten addition seemed to have just a weak effect on general corrosion [94].

3.3.4. Other electrolytes [95, 96]

The interaction between a low carbon steel and a fluorosilicate melt $K[Mg_3AlSi_3O_{10}]F_2$ was studied as a function of the immersion depth of the samples [95]. It was found that in the middle of the melt the corrosion rate was the highest due to the formation of a surface Fe + Si alloy resulting in a local corrosion galvanic cell (Fe + FeSi). The adsorption of potassium and magnesium ions seemed to have an inhibiting effect [95]. The corrosion losses of a Cr–Ni–Ti stainless steel in vanadate melts increased with the V_2O_5 content due to the reduction of the oxide to V^{4+} with a simultaneous oxygen release [96]. The activation energy of the process was 18 kJ mol^{-1} implying transport limitations. X-ray analysis of the surface showed that Fe_3O_4 and Cr_2O_3 were the principal scale constituents (scale thickness of the order of 10 μm [96]). The metal zone near the oxide interface was enriched with chromium.

4. Overview of hot-corrosion mechanisms

4.1. The fluxing model [98–104]

Hot corrosion can be identified by the degradation of metals or alloys in contact with a thin fused salt film in the presence of aggressive gases. Recently, the so-called oxide-scale fluxing model was proposed by Rapp and co-workers [98, 100–104] to explain the phenomenon. The essence of the model is that protective oxide scales formed by high-temperature oxidation are dissolved in, or penetrated by, fused salt. It was established [100–104] that the solubility of a range of oxides (Fe_2O_3, NiO, SiO_2, etc.) depended strongly on the melt basicity and so did the type of the dissolution mechanism. The process of rupture of the barrier oxide scale and the precipitation of the secondary porous oxide deposit from the salt film is presented schematically in Fig. 9 [98, 100–105].

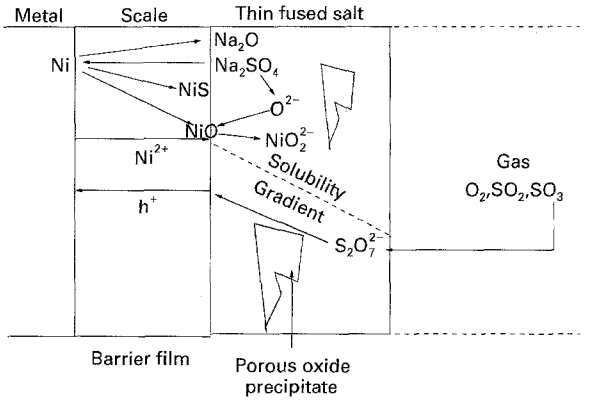

Figure 9 Basics of the fluxing model of the hot corrosion of nickel by thin fused sulphate films in aggressive SO_2, SO_3 atmospheres [105].

According to Rapp and Goto [98] the negative gradient of the oxide solubility in a thin fused salt film might establish self-sustained hot corrosion of the pure metal (Rapp–Goto criterion, Fig. 9). Reduction of dissolved SO_3 as $S_2O_7^{2-}$ was the main cathodic reaction during corrosion of preoxidized nickel covered with a thin Na_2SO_4 film in an SO_2–O_2 gas atmosphere [105]. Metal sulphidation via direct contact between the melt and nickel metal in combination with the above reduction, ensured a negative basicity gradient in the salt film resulting in a negative solubility gradient of NiO [105]. A conclusion was drawn that the self-sustaining corrosion of nickel in sulphate melts was only observed when the basicity and oxygen partial pressure at the oxide/melt interface corresponded to the basic dissolution regime for NiO [105].

An attempt to assess the mechanism of hot corrosion, emphasizing the changes in the system conductivity during the fluxing of the nickel oxide scale by molten salt, was made by Wu and Rapp [106] using a.c. impedance spectroscopy. Three distinctive reaction states were observed during the hot-corrosion process [106]: (1) a passive state corresponding to slight corrosion; (2) a pseudoactive state where passivity could be ended by a forced unstable condition (e.g. polarization); (3) an active state where hot corrosion occurred with no incubation time at all and provoked a severe destruction of the sample. In the passive state, a continuous NiO oxide film was assumed to be present at the metal surface; thus the total impedance of the system could be

$$Z_T = Z_{M/O} + Z_{ox} + Z_{O/S} \quad (30)$$

The corresponding physical picture of the system $Ni/NiO/Na_2SO_{4(melt)}/SO_{3(gas)}$ is presented in Fig. 10 [106]. The equivalent electrical circuit of the system [106] is also shown in the figure.

The following expressions were proposed for the components of the impedance function

$$Z_{M/O} = [j\omega C_{M/O} + 1/R_h]^{-1} \quad (31)$$

$$Z_{ox} = \{1/R'_h + j\omega C_{ox} + 1/[\sigma_M \omega^{-1/2}(1-j)]\} \quad (32)$$

$$Z_{O/S} = \{1/R''_h + j\omega C_{O/S} + 1/[R''_M + \sigma_0 \omega^{-1/2}(1-j)]\} \quad (33)$$

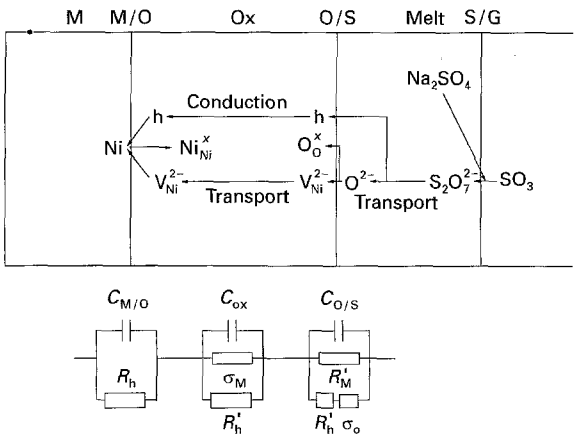

Figure 10 A model of the conductivity of the system nickel/oxide scale/thin molten salt film/gas during hot corrosion and the corresponding equivalent electrical circuit of the system [106].

where R_h, R'_h and R''_h are the charge transfer resistances of holes through the interfaces and the film (Fig. 10), R''_M is the charge transfer resistance of cation vacancies at the O/S interface and σ_0 is the Warburg constant of diffusion of $S_2O_7^{2-}$ in the molten salt film (Fig. 10). The Warburg constant of migration of cation vacancies through the film (Fig. 10) is given by

$$\sigma_M = (RT/4F^2)[1/(2D_M)^{1/2}c_{VM}] \quad (34)$$

where D_M is the diffusion coefficient of cation vacancies and c_{VM} the concentration of vacancies at the M/O interface (Fig. 10).

In the pseudo-passive state [106] the continuous NiO film was penetrated by molten salt and the overall impedance response was dominated by the finite diffusion impedance in the pores and flaws

$$Z_W = R_W[\tanh(j\omega\delta^2/D)^{1/2}/(j\omega\delta^2/D)^{1/2}] \quad (35)$$

where D is the diffusion coefficient of $S_2O_7^{2-}$ and δ the diffusion length. Because the pore dimensions were small compared to the salt film thickness, the pore diffusion of $S_2O_7^{2-}$ could be treated as bounded [106].

In the active state, the severe dissolution of nickel was tentatively explained by the following simplified model [106]

$$Ni + 2h' \rightarrow Ni^{2+} \quad (36)$$

$$Ni^{2+} + \tfrac{3}{2}O^{2-} + \tfrac{1}{4}O_2 \underset{k_b}{\overset{k_f}{\rightleftharpoons}} NiO_2^- \quad (37)$$

where k_f and k_b are the forward and backward rate constants. For this reaction sequence the theoretical impedance response for active hot corrosion was derived as [106]

$$\begin{aligned} Z_F = {} & R_{ct} + [K\sigma_0\omega^{-1/2}/(K+1)]\{[(g^2+1)^{1/2} \\ & - j(g^2+1)^{1/2} - g]^{1/2}/(g^2+1)^{1/2}\} \\ & + \sigma_0[1/(K+1)]\omega^{-1/2}(1-j) \\ & + \sigma_R\omega^{-1/2}(1-j) \end{aligned} \quad (38)$$

where $\sigma_O = R_{ct}/[2F(2D_O)^{1/2}\partial i_F/\partial C_O]$ and $\sigma_R = R_{ct}/[2F(2D_R)^{1/2}\partial i_F/\partial C_R]$ with $g = k/\omega$, $k = k_f + k_b$ and $K = k_f/k_b$. The diffusion length of the cathodic reaction was estimated to be 2 μm, a value reasonable for diffusion within or near the pores, using a diffusion coefficient for $S_2O_7^{2-}$ of 2×10^{-4} cm^2 s^{-1} [106]. As a conclusion, the authors [106] pointed out that although the obtained mechanistic information was valuable, it did not necessarily identify the rate-limiting step in the hot-corrosion reaction corresponding perhaps to a high-impedance step in parallel with a low-impedance step.

4.2. Influence of different factors on the mechanism of hot corrosion

4.2.1. Specimen purity

Specimen purity strongly affected the hot-corrosion behaviour of nickel in contact with molten sulphate films [105]. For essentially the same oxide thickness, the preoxidized samples of 99.99% Ni did not suffer

from sulphidation (Fig. 9) and thus only slight corrosion was observed in contrast to 99% Ni which was entirely transformed to NiO for identical times of measurement [105]. The oxide scale on the purer nickel was more perfect, no penetration of the salt film occurred and the surrounding gas atmosphere sustained the acidic dissolution regime. The conditions did not satisfy the Rapp–Goto criterion [98] because the solubility gradient was positive, the NiO saturated film was not expected to dissolve and the corrosion was slowed down. This conclusion was verified by Otsuka and Rapp [105] using more basic melts in contact with preoxidized 99.99% Ni.

4.2.2. Anion additives

In a further paper, Otsuka and Rapp [107] discussed the chromate anion addition in concentrations of less than 50 mol % which resulted in a more severe hot corrosion of nickel compared to pure Na_2SO_4 melts. This was attributed to a more favourable cathodic coupled reaction than that of $S_2O_7^{2-}$ reduction

$$2CrO_4^{2-} + O^{2-} \rightarrow 2CrO_4^{3-} + \tfrac{1}{2}O_2 \quad (39)$$

$$CrO_4^{3-} + e^- \rightarrow CrO_3^{2-} + O^{2-} \quad (40)$$

For melts containing 50 mol % chromate, the solubility of Cr_2O_3 was exceeded and its precipitation occurred according to the reaction

$$2CrO_4^{2-} + 2SO_3 \rightarrow Cr_2O_3 + \tfrac{3}{2}O_2 + 2SO_4^{2-} \quad (41)$$

This precipitation, if abundant, could block the reactive sites in the protective oxide scale and thereby isolate the salt from the base metal (the analogous mechanism is generally accepted for chromate inhibition in aqueous corrosion) [107]. This mechanism could prove useful in explaining the influence of chromium in Ni–Cr alloys as follows: chromium oxide in the scale dissolved on contact with sulphate melts, providing anions to prevent the abrupt rise of the basicity of the salt film [107]. At locally reduced sites of the scale, however, chromate could precipitate as Cr_2O_3 and inhibit the salt/metal contact and sulphidation of the base metal. Such backward precipitation was noted as the "inverse Rapp–Goto effect" [107].

Vanadate addition, conversely, enhanced the onset of hot corrosion due, most probably, to the higher solubility of most oxides in the mixed fused sulphate–vanadate solution [107]. Therefore, the acidic dissolution of scales proceeded to an early salt/metal contact at defects (cracks and/or grain boundaries) in the protective oxide. Thus, the major condition for the pronounced detrimental effect of vanadate was the existence of flaws and imperfections in the oxide film – for scales grown on high-purity nickel no enhancement of hot corrosion by vanadate was observed [107].

4.2.3. Effect of aggressive gases – low-temperature hot corrosion [109, 110]

This type of corrosion resulted from the formation of molten $MeSO_4$–Na_2SO_4 (melting points 500–700 °C) by reaction of SO_3 with oxide scales and surface salt deposits [110]

$$NiO + SO_3 \rightarrow NiSO_4 \quad (42)$$

$$NiSO_4 + Na_2SO_4 \rightarrow NiSO_4\text{–}Na_2SO_4 \text{ (mixed sulphates)} \quad (43)$$

Mixed sulphates of the α-$Na_2Ni(SO_4)_2$ type and excess NiO were identified by X-ray diffraction [110]. In pure SO_2 atmosphere, the catalytic activity of NiO and Co_3O_4 scales was sufficient to produce appreciable SO_3 content, entailing the mixed sulphate formation as rapidly as in the equilibrium of SO_3 provided. The possible formation of molten ternary sulphates was also foreseen [110] because it would lead to melting at lower temperatures and larger amounts of molten sulphates at a given pressure of SO_3. The corrosion of nickel in molten $NiSO_4$–Na_2SO_4 occurred mainly via formation of liquid sulphide (presumably Ni_3S_2–Ni eutectic) below the surface oxide (see Fig. 9). Liquid sulphate was suggested [110] to penetrate the surface oxide and react with the underlying metal

$$9Ni + NiSO_4 \rightarrow 8NiO + Ni_3S_2 \quad (44)$$

or SO_3 to diffuse into the NiO–Ni interface and react there [110]

$$2SO_3 + 9Ni \rightarrow 6NiO + Ni_3S_2 \quad (45)$$

4.2.4. Effect of the molten salt type (hot corrosion in carbonates) [111, 112]

Hot corrosion of iron in contact with thin fused Li_2CO_3–K_2CO_3 under O_2–CO_2 atmospheres was defined by plotting phase stability diagrams of the Li–Fe–K–C–O system [111]. The corrosion rate followed a parabolic law with a constant of $2.7 \times 10^{-9}\ g^2\,cm^{-4}\,s^{-1}$. XRD analysis indicated that the porous outer corrosion layer was composed of Fe_2O_3 and $LiFe_5O_8$ corresponding to the thermochemical calculations [111]. The inner barrier film consisted of FeO and Fe_3O_4 whose growth was controlled by the outward cation diffusion [111]. The increased CO_2 concentration from 0.01% to 10% resulted in corrosion inhibition and an outer layer of FeO and $Li_2Fe_3O_5$ [111].

An attempt to apply the Rapp–Goto theory to hot corrosion of nickel in molten carbonates under $O_2 + CO_2$ atmospheres was presented by Lee and Shores [112]. Several reaction steps were considered taking into account the possible formation of both peroxide and superoxide ions [112]. Thus for Li^+-rich melts (peroxide formation)

$$Ni + O_2^{2-} \rightarrow Ni^{2+} + 2O^{2-} \text{ (in acidic melts)} \quad (46)$$

$$Ni + O_2^{2-} \rightarrow NiO_2^{2-} \text{ (in basic melts)} \quad (47)$$

$$Ni + O_2^{2-} \rightarrow NiO + O^{2-} \quad \text{(in saturated melts)} \tag{48}$$

and for K^+-rich melts (superoxide formation)

$$Ni + O_2^- \rightarrow Ni^{2+} + O^{2-} + O_2 \quad \text{(in acidic melts)} \tag{49}$$

$$Ni + 2O_2^- \rightarrow NiO_2^{2-} + O_2 \quad \text{(in basic melts)} \tag{50}$$

On the basis of steady state flux of dissolved NiO it was suggested [112] that fluxing was sustained even by a moderate solubility gradient, thus the Rapp-Goto criterion was satisfied and a negative solubility gradient was the cause of the non-protective oxidation behaviour of nickel in molten carbonates [112]. The oxidation process was divided into three stages, fluxing and dissolution of NiO being the rate-limiting step in the first one (incubation period) [112]. X-ray diffraction confirmed the formation of $LiNiO_2$ in the melt [112]. In the acceleration period (stage II [112]) the transport of oxidant and/or dissolved NiO was assumed to be rate-determining [112]. In the linear period of oxidation (stage III [112]) the oxidation rate being virtually independent of pCO_2 and the salt composition, it was suggested [112] that the oxygen dissolution reaction became the rate-limiting step (the linear dissolution rate was found to be roughly proportional to pO^{2-} [112].

4.2.5. Effect of alloying elements – mechanism of hot corrosion of nickel superalloys [113–118]

The problem of the hot-corrosion attack of gas turbine components exposed to combustion gases is encountered under circumstances where air and fuel are contaminated with salts. Most nickel-based superalloys are susceptible to hot corrosion because their oxidation resistance is due to a continuous oxide layer of α-Al_2O_3 adjacent to the metal substrate. Hot corrosion is a localized attack starting at single sites and spreading laterally on the samples.

A schematic representation of the kinetic curve of a nickel superalloy in thin Na_2SO_4 and O_2, SO_2/SO_3-containing atmosphere is presented in Fig. 11 [115–118]. The various identified oxidation periods are outlined in the figure. During the induction period 1 (0–3 h), oxidation and dissolution of chromium oxide, dissolution of TiO_2 in the scale, took place and molybdenum oxide was formed by oxidation of surface carbides with the simultaneous release of SO_3 [115, 116]

$$Cr_2O_3 + \tfrac{3}{2}O_2 + 2Na_2SO_4 \rightarrow 2Na_2CrO_4 + 2SO_3\uparrow \tag{51}$$

$$nTiO_2 + 2Na_2SO_4 \rightarrow 2Na_2O(TiO_2)_n + \tfrac{1}{2}O_2 + 2SO_2\uparrow \tag{52}$$

$$MoO_3 + 2Na_2SO_4 \rightarrow 2Na_2MoO_4 + 2SO_3\uparrow \tag{53}$$

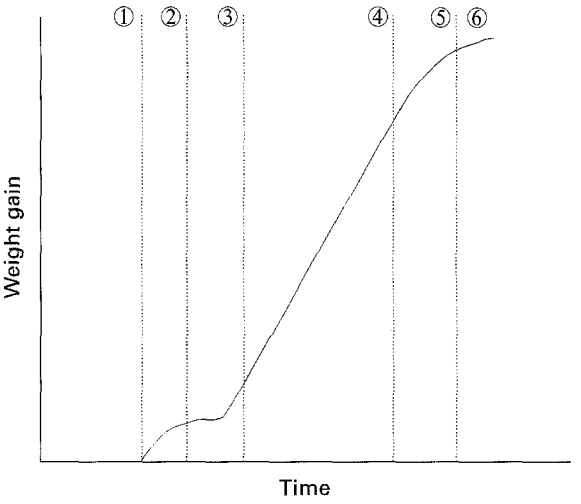

① Induction period
② First parabolic region (basic fluxing)
③ Intermediate region (liquid MoO_4^{2-} formation)
④ Linear region (acidic fluxing)
⑤ Deceleration region (liquid $NiMoO_4$ formation)
⑥ Second parabolic region (basic fluxing)

Figure 11 Schematic representation of the kinetic curve of hot corrosion of a nickel superalloy in thin molten salt film under aggressive SO_2, SO_3 atmospheres [115].

At the end of the induction period, the sulphate ions began to penetrate through the oxide scale and convert alloy constituents to sulphides and oxides [115]

$$Ni + SO_4^{2-} \rightarrow NiS + \tfrac{3}{2}O_2 + O^{2-} \tag{54}$$

$$2Al + 3SO_4^{2-} \rightarrow Al_2O_3 + 3SO_3 + 3O^{2-} \tag{55}$$

$$2Cr + 3SO_4^{2-} \rightarrow Cr_2O_3 + 3SO_3 + 3O^{2-} \tag{56}$$

leading to an increase of melt basicity up to a value at which the Rapp–Goto criterion was satisfied [98]. Such an increase resulted in the basic fluxing of the aluminium oxide scale (first parabolic region 2, Fig. 11)

$$Al_2O_3 + O^{2-} \rightarrow 2AlO_2^- \tag{57}$$

Reprecipitation of aluminium and chromium oxides in the intermediate region 3 (9–10 h) was provoked by the consumption of oxide ions in the melt by liquid MoO_3

$$MoO_3 + O^{2-} \rightarrow MoO_4^{2-} \tag{58}$$

$$2NaAlO_2 + MoO_3 \rightarrow Al_2O_3 + Na_2MoO_4 \tag{59}$$

$$2Na_2CrO_4 + 2MoO_3 \rightarrow Cr_2O_3 + 2Na_2MoO_4 + \tfrac{3}{2}O_2 \tag{60}$$

Sodium molybdate tended to stabilize the molten molybdate/molybdenum oxide phase [115].

In the beginning of the linear oxidation region 4 (Fig. 11) most of the sulphate reacted and the corrosive molten phase was largely Na_2MoO_4/MoO_3 effectuating the acidic fluxing of the aluminium and chromium protective oxides

$$Al_2O_3 + MoO_3 \rightarrow 2Al^{3+} + 3MoO_4^{2-} \tag{61}$$

$$Cr_2O_3 + MoO_3 \rightarrow 2Cr^{3+} + 3MoO_4^{2-} \tag{62}$$

The self-sustaining feature of the acidic fluxing was obtained by the cyclic operation of these two reactions and their reverses. A layered appearance of the oxide scale was produced and its disruption took place, thus allowing the oxygen penetration and oxidation of nickel sulphides formed at the end of the induction period

$$NiS + \tfrac{3}{2}O_2 \rightarrow NiO + SO_2 \quad (63)$$

If hot corrosion was induced by a molten sulphate layer of a smaller thickness, the deceleration of the linear rate 5 proceeded due to liquid MoO_3 conversion to a solid salt [115, 117]

$$NiO + MoO_3 \rightarrow NiMoO_4 \quad (64)$$

The increase of the solid content in the liquid + solid layer reduced the transport rate [117]. That resulted in a decreased rate of alloy consumption and MoO_3 formation, the molten molybdate film evaporated gradually and the rate of corrosion resembled that of pure oxidation (second parabolic region 6, Fig. 11). A similar effect on hot corrosion was observed for tungsten (WO_3 and Na_2WO_4, and respectively $NiWO_4$ [116]).

Fig. 12 illustrates the changes in the phase composition and structure of the alloy/scale/melt/gas system during the oxidation whose kinetics is depicted in Fig. 11 [115–118]. For the sake of simplicity, the reprecipitation of aluminium and chromium from molten sulphate/molybdate and the evolution of SO_2 and SO_3 are not illustrated in the figure. Also, the

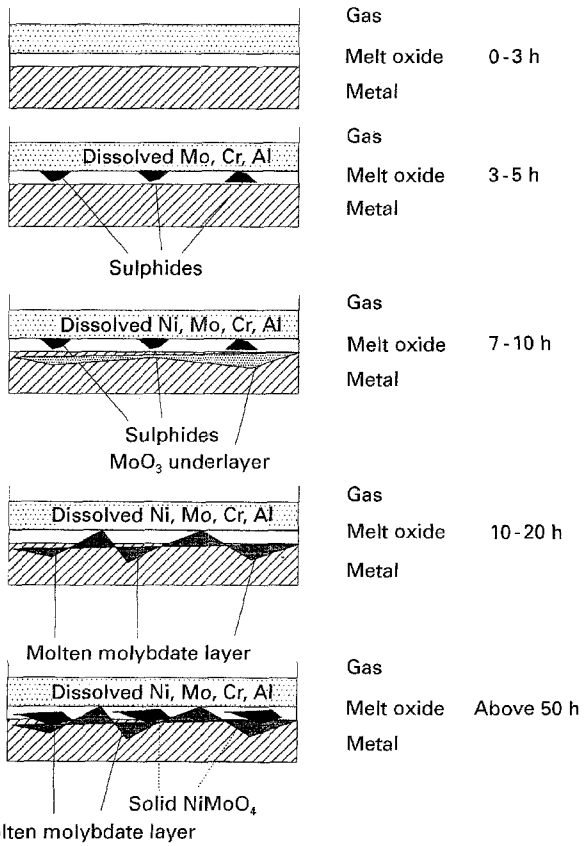

Figure 12 Schematic representation of the changes in the phase composition and structure of the system alloy/scale/melt/gas during hot corrosion as deduced from EDAX and X-ray results [115, 116].

effect of some minor constituents of the alloys such as tantalum and niobium, is not outlined. The impact of these elements ensues from the prolonging of the induction period due to the reaction with Na_2SO_4

$$Ta_2O_5 + Na_2SO_4 \rightarrow 2NaTaO_3 + SO_3\uparrow \quad \text{(similarly for niobium)} \quad (65)$$

increasing the acidity of the melt and preventing basic fluxing, on the one hand (Fig. 11) and bonding sodium into a high-melting compound, reducing the formation of Na_2MoO_4 and limiting the acidic fluxing, on the other. Furthermore, tantalum and niobium acted as a sink for Na_2O [116] in the deceleration period.

5. Conclusions

A comprehensive review of the corrosion and anodic behaviour of nickel, iron, cobalt and alloys thereof, in molten salt-based electrolytes, is presented emphasizing the reaction mechanisms. The following general conclusions can be drawn from the overview.

1. Most of the recent literature on the problem deals with the corrosion behaviour of nickel as one of the metals most resistant to corrosion in molten salts. However, a few detailed mechanisms were presented and mainly steady state electrochemical techniques combined with surface analysis were used to elucidate the reaction kinetics and the type of corrosion products. Corrosion layers formed on nickel were most often identified with NiO, higher oxides of the spinel and haematite type being not unanimously detected. Passivation was observed both in halide melts containing oxygen and in melts with oxoacid counterions, but a mechanism of passive film growth and dissolution was advanced in nitrate melts only. No transient techniques were applied to the study of the corrosion and anodic behaviour of nickel in melts.

2. Studies of iron and especially cobalt corrosion in molten salts in the last two decades are scarce. Once again, mostly stationary measurements (weight loss/gain, d.c. polarization and open-circuit potential registration) were carried out to assess the reaction mechanisms. There is no unanimity on the composition of both the corrosion layers and the secondary soluble corrosion products of iron. Passivation of iron was thought to be diffusion-limited, and the growth of the passive film obeyed the high-field transport mechanism. Cobalt was found to be the least susceptible to passivation and its passivation reaction was qualified as reversible.

3. From literature data, the picture of the influence of major and minor alloying elements on the corrosion resistance and anodic behaviour of nickel, iron- and cobalt-based alloys is fairly incomplete. Most of the investigations are purely empirical and a systematic investigation of the impact of additives has been attempted in a few cases only. A general conclusion is that alloying with chromium leads to the formation of strongly protective corrosion layers based on chromium oxides and/or sulphides. Alloys forming surface films based on the main metal (nickel, iron or cobalt oxides, mixed oxides, etc.) are more susceptible to corrosion. The addition of alloying elements which are

subject to oxidation, permits the acid fluxing of the oxide scale (molybdenum, tungsten, vanadium, niobium, etc.) and has a detrimental effect on the corrosion resistance of alloys in molten salt media.

4. The chemical background and basic kinetics of hot corrosion of nickel, iron, cobalt and their alloys is qualitatively well-defined, especially in recent years' work. The fluxing model and the Rapp–Goto criterion of oxide solubility have been generally accepted and are widely used to estimate the corrosion susceptibility of metals and alloys in thin molten salt films. There were, however, a few attempts to use electrochemical thin film techniques and namely transient ones, in the study of hot-corrosion processes, and also most of the information concerning chemical, structural and morphological aspects of hot corrosion has come from *ex situ* surface analysis studies.

These general conclusions enable the suggestion of some future trends of investigation in the field.

1. There is a significant need to employ transient methods (a.c. impedance, pulse measurements, controlled hydrodynamic methods such as the rotating disc electrode, etc.) in the study of corrosion and anodic oxidation processes of metals in molten salt media. It will enable us to gain a deeper insight into the individual steps of reactions coupled in the corrosion process.

2. A systematic study of the influence of the main alloying elements in nickel-based alloys and stainless steels (chromium, molybdenum, tungsten etc.) would be of great help to the subsequent optimization of the alloy composition and pretreatment conditions in order to improve their corrosion resistance to such corrosive media as molten salts containing oxidizing agents.

Acknowledgement

The authors are grateful to the National Scientific Research Fund, Ministry of Science and Education, for the financial support of this work.

References

1. J. A. PLAMBECK, in "Encyclopedia of the electrochemistry of the elements", Vol. X, edited by Allen J. Bard (Marcel Dekker, New York, 1976)
2. J. DUBOIS and R. BUVET, *Bull. Soc. Chim. Fr.* **408** (1963) 2522.
3. M. D. INGRAM and G. J. JANZ, *Electrochim. Acta* **10** (1965) 783.
4. A. CONTE and S. CASADIO, *Ricerca Scient.* **36** (1966) 488.
5. A. CONTE and M. D. INGRAM, *Electrochim. Acta* **13** (1968) 1551.
6. S. L. MARCHIANO and A. J. ARVIA, *ibid.* **17** (1972) 861.
7. G. BOMBARA, G. BAUDO and A. TAMBA, *Corros. Sci.* **8** (1968) 393.
8. C. A. C. SEQUEIRA and M. G. HOCKING, *Br. Corros. J.* **12** (1977) 158.
9. L.M. GRIBAUDO and J. J. RAMEAU, *Rev. Int. Hautes Temp. Refract.* **20** (1983) 89.
10. A. RAHMEL, *Electrochim. Acta* **13** (1968) 495.
11. G. BAUDO and A. TAMBA, *Br. Corros. J.* **4** (1969) 129.
12. R. DOISNEAU and B. TREMILLON, *Bull. Soc. Chim. Fr.* **420** (1976) 1419.
13. G. S. PICARD, H. M. LEFEBVRE and B. TREMILLON, *J. Electrochem. Soc.* **134** (1987) 52.
14. J. AMOSSE, J. BOUTEILLON and M. J. BARBIER, *C.R. Acad. Sci. Ser. C* **276** (1968) 22.
15. J. BOUTEILLON and M. J. BARBIER, *J. Electroanal. Chem.* **56** (1974) 399.
16. C. H. LIU, A. J. ZIELEN and D. M. GRUEN, *J. Electrochem. Soc.* **120** (1973) 67.
17. R. COMBES, J. VEDAL and B. TREMILLON, *J. Electroanal. Chem.* **27** (1970) 174.
18. V. KOCHERGIN, O. PUTINA, V. DEVYATKIN and E. KANAEVA, *Prot. Met.* **11** (1975) 224.
19. D. FERRY, G. PICARD and Y. CASTRILLEJO, *J. Appl. Electrochem.* **23** (1993) 735.
20. X. FENG and C. A. MELENDRES, *J. Electrochem. Soc.* **129** (1982) 1245.
21. A. ZHBANOV, A. VOLKOVICH, A. VINOGRADOV, B. KOVALEV and A. VENGERENKO, *Izv. VUZ Tsvet. Met.* **2** (1981) 29.
22. A. NISHIKATA and S. HARUYAMA, *Corros. NACE* **42** (1986) 578.
23. A. J. ARVIA, R. C. V. PIATTI and J. J. PODESTA, *Electrochim. Acta* **17** (1972) 901.
24. J. J. PODESTA, R. C. V. PIATTI and A. J. ARVIA, *Corros. Sci.* **17** (1977) 225.
25. A. BARAKA and S. BARAKA, *J. Appl. Electrochem.* **14** (1984) 305.
26. *Idem, ibid.* **14** (1984) 417.
27. P. PRASAD and P. JENA, *Metall. Trans.* **2** (1971) 1651.
28. J. QUETS and W. H. DRESHER, *J. Mater. JMSA* **4** (1969) 583.
29. K. E. JOHNSON and H. A. LAITINEN, *J. Electrochem. Soc.* **110** (1963) 314.
30. G. BAUDO, A. TAMBA and G. BOMBARA, *Corros. NACE* **26** (1970) 193.
31. S. PIZZINI and L. AGACE, *Corros. Sci.* **5** (1965) 193.
32. F. MANSFELD, N. E. PATON and W. M. ROBERTSON, *Metall. Trans.* **4** (1973) 321.
33. A. RAHMEL, *Chem. Eng. Technol.* **41** (1969) 169.
34. E. TACHAR-MOISESCU and A. RAHMEL, *Electrochim. Acta.* **20** (1975) 479.
35. C. A. C. SEQUEIRA and B. HOCKING, *ibid.* **8** (1978) 145.
36. *Idem, ibid.* **8** (1978) 179.
37. G. M. ABOU-ELENIEN, *J. Appl. Electrochem.* **21** (1991) 632.
38. G. J. JANZ and P. SAEGUSA, *Electrochim. Acta* **7** (1962) 393.
39. P. DEGOBERT and O. BLOCH, *Bull. Soc. Chim. Fr.* **407** (1962) 1887.
40. K. Y. KIM and O. F. DEVEREUX, *Corros. Sci.* **22** (1982) 22.
41. O. F. DEVEREUX, *Corros. NACE* **35** (1979) 125.
42. O. F. DEVEREUX and K. Y. KIM, *ibid.* **36** (1980) 262.
43. O. F. DEVEREUX, K. Y. KIM and K. S. YEUM, *Corros. Sci.* **23** (1983) 205.
44. N. IYER and O. F. DEVEREUX, *J. Electrochem. Soc.* **132** (1985) 1098.
45. G. JANZ and A. CONTE, *Electrochim. Acta* **9** (1964) 1269.
46. *Idem, ibid.* **9** (1964) 1279.
47. H. J. DAVIS and D. K. KINNIBRUGH, *J. Electrochem. Soc.* **117** (1970) 392.
48. G. SMITH, *Oak Ridge National Lab.* **15** (1957) 2129.
49. *Idem, Trans. AIME* **2** (1956) 71.
50. A. KOLOTIJ and G. VENGZHEN, *Prot. Met.* **11** (1975) 61.
51. V. BUDNIK and O. ZARUBITSKIJ, *Zh. Prikl. Khim.* **7** (1975) 1628.
52. TZ. TZVETKOFF and R. RAICHEFF, in "34th ISE Meeting", Erlangen, 1983, Extended Abstracts, 0628.
53. TZ. TZVETKOFF and I. IVANOV, "Electrochemical Methods in Corrosion Research" (Toulouse, 1985) Extended Abstracts, p. 44.
54. B. DMITRUK, N. BABICH and O. ZARUBITSKIJ, *Ukr. Khim. Zh.* **52** (1986) 728.
55. A. RAHMEL and H. KRUGER, *Werkst. Korros.* **18** (1967) 193.
56. S. M. TIN'KOVA, V. V. SKORODUMOV, I. A. KUPRJAKOVA and V. T. GONDAREV, *Izv. VUZ Tsvet. Met.* **1** (1978) 141.

57. C. T. LIU and O. F. DEVEREUX, *J. Electrochem. Soc.* **131** (1984) 247.
58. M. JUT and O. USTINOV, *Prot. Met.* **14** (1978) 320.
59. E. MATJUSHIN and O. USTINOV, *ibid.* **14** (1978) 59.
60. D. L. MANNING, *J. Electroanal. Chem.* **6** (1963) 227.
61. *Idem, ibid.* **7** (1964) 302.
62. S. PIZZINI, M. MORLOTTI and E. ROMER, *J. Electrochem. Soc.* **113** (1966) 2305.
63. A. ROBIN and J. DE LEPINAY, *Electrochim. Acta* **37** (1992) 2433.
64. V. KOCHERGIN, I. VINIARSKAJA and YU. KOVALEV, *Prot. Met.* **12** (1976) 79.
65. H. LAITINEN and C. H. LIU, *J. Am. Chem. Soc.* **80** (1958) 1015.
66. M. V. SMIRNOV, A. V. POKROVSKIJ and N. A. LOGINOV, *Zh. Neorg. Khim.* **15** (1970) 3154.
67. V. A. DUBININ, I. F. NICHKOV and S. P. RASPOPIN, *Izv. VUZ Tsvet. Met.* **9** (1966) 73.
68. L. G. BOXALL, H. L. JONES and R. A. OSTERYOUNG, *J. Electrochem. Soc.* **121** (1974) 212.
69. TZ. TZVETKOFF, in "35th ISE Meeting", Berkeley, USA (1984) Extended Abstracts, A5, p. 293.
70. A. J. ARVIA, J. J. PODESTA and R. C. V. PIATTI, *Electrochim. Acta* **17** (1972) 33.
71. J. C. STEMMELIN, L. A. SUAREZ-INFANZON and J. BRENET, *C.R. Acad. Sci. Ser. C* **265** (1967) 141.
72. M. E. MARTINS, A. S. CALANDRA and A. J. ARVIA, *J. Inorg. Nucl. Chem.* **36** (1974) 1705.
73. A. J. ARVIA, J. J. PODESTA and R. C. V. PIATTI, *Electrochim. Acta* **16** (1971) 1797.
74. D. G. HILL, B. PORTER and A. S. GILLESPIE, *J. Electrochem. Soc.* **105** (1958) 408.
75. A. CASINO, J. J. PODESTA and A. J. ARVIA, *Electrochim. Acta* **16** (1971) 121.
76. D. D. WILLIAMS, J. A. GRAND and R. R. MILLER, *J. Am. Chem. Soc.* **78** (1956) 5150.
77. A. KOZHEMJAKO, V. PRISJAZHNIJ, D. TKALENKO and V. MNIKH, *Prot. Met.* **22** (1986) 984.
78. TZ. TZVETKOFF, in "36th ISE Meeting", Salamanca, Spain (1986) Extended Abstracts CI, p. 171.
79. M. AZZI and J. J. RAMEAU, *Corros. Sci.* **24** (1984) 435.
80. I. OZERJANAJA, A. FINKELSTEIN, T. MANUKHINA, O. PENJAGINA and V. SMIRNOV, *Prot. Met.* **3** (1967) 581.
81. V. KOCHERGIN and A. KOKUROVA, *Zh. Neorg. Khim.* **7** (1962) 1331.
82. G. JANZ and A. CONTE, *Corros. NACE* **20** (1964) 237.
83. O. PENJAGINA, I. OZERJANAJA and N. SHAMANOVA, *Prot. Met.* **17** (1981) 460.
84. *Idem, Trudy Inst. Elektrokhim. UNT AN USSR* **24** (1976) 39.
85. S. W. ORCHARD and G. MAMANTOV, *J. Electrochem. Soc.* **136** (1989) 3565.
86. V. BELOV, T. ERSHOVA and V. KOCHERGIN, *Ukr. Khim. Zh.* **44** (1978) 581.
87. G. DMITRIEVA, O. KOSTYRKO, I. MAKSJUTA, N. RAZUMOVA and A. SHURIN, *Prot. Met.* **23** (1987) 316.
88. H. ATMANI and J. J. RAMEAU, *Corros. Sci.* **24** (1984) 279.
89. A. BARAKA, A. ABDEL ROHMAN and A. EL-HOSARY, *Br. Corros. J.* **11** (1976) 44.
90. R. DOELLING, H. HOLTAN, A. STERLEN and R. TUNOLD, *Werkst. Korros.* **31** (1980) 470.
91. F. NIJGER, I. OZERJANAJA, V. BEZHENAR and R. MARUSJAK, *Prot. Met.* **18** (1982) 75.
92. W. SCHENDLER and W. SCHWENK, *Werkst. Korros.* **32** (1981) 1428.
93. E. ERDOES, H. ALTORFER and E. DENZLER. *ibid.* **33** (1982) 373.
94. L. M. GRIBAUDO and J. J. RAMEAU, *Corros. Sci.* **24** (1984) 291.
95. V. GOLENKO and V. PUTILIN, *Prot. Met.* **17** (1981) 572.
96. M. FAZLEEV and A. FEDOROV, *ibid.* **18** (1982) 448.
97. D. INMAN and N. S. WRENCH, *Br. Corros. J.* **1** (1966) 246.
98. R. A. RAPP and K. S. GOTO, in "Molten Salts", Vol. 81–10, edited by J. Braunstein and J. R. Selman (Electrochemical Society Softbound Proceedings Series, Pennington, NJ, 1981) p. 159.
99. D. A. SHORES, in "High Temperature Corrosion", NACE-6, edited by R. A. Rapp, (National Association of Corrosion Engineers, Houston, TX, 1983) p. 493.
100. C. O. PARK and R. A. RAPP, *J. Electrochem. Soc.* **133** (1986) 1636.
101. R. A. RAPP, *Corrosion* **42** (1986) 568.
102. *Idem, Mater. Sci. Eng.* **87** (1987) 319.
103. Y. S. ZHANG and R. A. RAPP, in "Molten Salts", Vol. 87–7, edited by G. Mamantov, M. Blander, C. Hussey, C. Mamantov, M. Saboungi and J. Wilkes (Electrochemical Society Softbound Proceedings Series, Pennington, NT, 1987) p. 707.
104. R. A. RAPP, in "Selected Topics on High Temperature Chemistry", edited by O. Johannesen and A. G. Anderson (Elsevier, New York, 1989) p. 291.
105. N. OTSUKA and R. A. RAPP, *J. Electrochem. Soc.* **137** (1990) 46.
106. Y. M. WU and R. A. RAPP, *ibid.* **138** (1991) 2683.
107. N. OTSUKA and R. A. RAPP, *ibid.* **137** (1990) 53.
108. Y. S. ZHANG and R. A. RAPP, *Corrosion* **43** (1987) 348.
109. K. L. LUTHRA and D. A. SHORES, *J. Electrochem. Soc.* **127** (1980) 2202.
110. R. L. JONES and S. T. GADOMSKI, *ibid.* **129** (1982) 1613.
111. H. S. HSU, J. H. DEVAN and M. HOWELL, *ibid.* **134** (1987) 3038.
112. K. N. LEE and D. A. SHORES, *ibid.* **137** (1990) 859.
113. D. M. JOHNSON, D. P. WHITTLE and J. STRINGER, *Corros. Sci.* **15** (1975) 649.
114. *Idem, ibid.* **15** (1975) 721.
115. G. C. FRYBURG, F. J. KOHL, C. A. STEARNS and W. L. FIELDER, *J. Electrochem. Soc.* **129** (1982) 571.
116. G. C. FRYBURG, F. J. KOHL and C. A. STEARNS, *ibid.* **131** (1984) 2985.
117. A. K. MISRA, *ibid.* **133** (1986) 1029.
118. *Idem. ibid.* **133** (1986) 1038.

Received 24 July 1994
and accepted 14 March 1995